nanomaterials

MDPI

Article

TiO_2 Nanoparticles/Nanotubes for Efficient Light Harvesting in Perovskite Solar Cells

Hwa-Young Yang [1,†], Won-Yeop Rho [2,†], Seul Ki Lee [1], Sang Hoon Kim [1] and Yoon-Bong Hahn [1,*]

1 School of Semiconductor and Chemical Engineering, Solar Energy Research Center, Chonbuk National University, Jeollabuk-do 54896, Korea; shot7108@gmail.com (H.-Y.Y.); kalyber@naver.com (S.K.L.); semikim77@gmail.com (S.H.K.)

2 School of International Engineering and Science, Chonbuk National University, 567 Baekje-daero, Deokjin-gu, Jeonju-si, Jeollabuk-do 54896, Korea; rho7272@jbnu.ac.kr

* Correspondence: ybhahn@chonbuk.ac.kr; Tel.: +82-63-270-2439

† These authors contributed equally to this work.

Received: 18 January 2019; Accepted: 20 February 2019; Published: 1 March 2019

Abstract: To enhance the light harvesting capability of perovskite solar cells (PSCs), TiO_2 nanoparticles/nanotubes (TNNs) were incorporated into the active layer of PSCs. The TNN-containing cells showed a substantial increase in photocurrent density (J_{SC}), from 23.9 mA/cm^2 without nanotubes to 25.5 mA/cm^2, suggesting that the TiO_2 nanotubes enhanced the charge conduction and harvested more sunlight, which was attributed to the Mie scattering effect. Compared to the power conversion efficiency (PCE) of TiO_2 nanoparticles in the active layer (14.16%), the TNN-containing cells with optimal loading of 9 wt % TiO_2 nanotubes showed a high PCE of 15.34%.

Keywords: perovskite solar cells; TiO_2 nanotube arrays; anodization; light harvesting

1. Introduction

Since Miyasaka introduced organometal halide perovskites into solar cells in 2009, perovskite solar cells (PSCs) have been a hot research topic in next-generation solar cells due to their capacity for absorption across a wide range of visible light [1–13]. Perovskite consists of Pb, methylammonium, and halide in a cubic structure with a tolerance factor (t) of 0.87–1.0 [6,14–18]. The structure of a perovskite solar cell consists of transparent conducting oxide (TCO), a compact layer, electron transport materials (ETMs), perovskite, hole-transport materials (HTMs), and a top electrode [19–25]. To improve energy conversion efficiency, zero-dimensional TiO_2 nanoparticles have been used as ETMs in perovskite solar cells and dye-sensitized solar cells due to the presence of a large band gap semiconductor and a large surface area [9,26–29]. Recently, perovskite stability, Au-free back electrodes, Pb-free sensitizers, various additives, additive-free HTMs, large-area modules, and Indium tin oxide (ITO)/Fluorine-doped tin oxide (FTO)-free devices have been studied substantially [1,3,5,30–35]. The structure of perovskite is ABX_3, which is very weak under humidity, heat, light, and oxygen. To enhance resistance to moisture [30,36], lead (Pb) is replaced by tin (Sn) for a Pb-free sensitizer [37]. To ensure device performance, additives are generally required in HTMs. However, the organic additives reduce the stability of PSCs, and thus they are replaced by metal oxides for long-term stability. Furthermore, the electron transport of zero-dimensional TiO_2 nanoparticles is no better than that of higher-dimensional TiO_2 nanostructures. It has been reported that TiO_2 nanotubes are useful in dye-sensitized solar cells to improve electron transport or to enhance light harvesting because they are three-dimensional nanostructures [38–42]. In general, TiO_2 nanotubes are prepared using

hydrothermal or electrochemical methods. In hydrothermal methods, many individual TiO_2 nanotubes are synthesized. However, in the electrochemical method, also called anodization, highly ordered and well-aligned TiO_2 nanotubes are synthesized. The size, length, thickness, and width of the TiO_2 nanotubes can be easily controlled on micron and nanometer scales as a function of reaction time, voltage, and concentration of electrolytes [43–50].

There are two light scattering theories from Rayleigh and Mie. Rayleigh scattering theory is applicable to small-sized particles, and Mie scattering theory, proposed by German physicist Gustav Mie, is applicable to large-sized particles. According to the Rayleigh theory, scattering by TiO_2 nanoparticles (20–30 nm) in the active layer is very weak. However, according to Mie scattering theory, submicrometer-sized TiO_2 nanoparticles are used effectively in the light scattering layer [51–54]. Individual TiO_2 nanotubes synthesized by a hydrothermal method are not suitable for light scattering, but the flakes of TiO_2 nanotubes synthesized by anodization are suitable for light scattering according to the Mie scattering theory. In this study, TiO_2 nanotube arrays were prepared by anodization and applied for perovskite solar cells (PSCs). To enhance the light harvesting capability of PSCs, TiO_2 nanoparticles/nanotubes (TNNs) were incorporated into the active layer of PSCs. The TNN-containing cells showed a substantial increase in photocurrent density (J_{SC}), suggesting that the TiO_2 nanotubes enhanced the charge conduction and harvested more sunlight, which is attributed to the Mie scattering effect.

2. Materials and Methods

2.1. Synthesis of TiO_2 Nanotube Arrays

A Ti plate was cleaned with water, ethanol, and acetone several times using a sonicator and was then dried. The anodization of the Ti plates was carried out in an electrolyte composed of 0.8 wt % NH_4F and 2 vol % H_2O in ethylene glycol at 25 °C at a constant applied voltage of 60 V. The TiO_2 nanotube arrays on the Ti plates were sintered at 500 °C for 1 h under ambient conditions to improve their crystallinity. To obtain free-standing TiO_2 nanotube arrays, a secondary anodization was carried out at a constant applied voltage of 30 V DC for 10 min, and then the Ti plates were immersed in a 10% H_2O_2 solution for 20 min.

2.2. Synthesis of Methylammonium Iodide and Preparation of Perovskite Solution

Methylammonium iodide (MAI) was synthesized using a methylamine solution (33 wt % in ethanol) and hydroiodic acid (57 wt % in water). First, methylamine was stirred using a dropwise addition of hydroiodic acid in an ice bath for 2 h. The solvent was evaporated by a rotary evaporator, and then the mixture was solvated in ethanol. After recrystallization with diethyl ether, the white solid was precipitated and then dried under a vacuum for 24 h. The perovskite solution was prepared with MAI and lead (II) chloride (99.999%, Sigma-Aldrich, St. Louis, MO, USA) at a 3:1 molar ratio, 45 wt %, in *N*,*N*-dimethylformamide (DMF).

2.3. Fabrication of the Perovskite Solar Cells

Figure 1A shows the schematic fabrication process of the PSCs incorporating TiO_2 nanotubes into the active layer. First, the compact layer of TiO_2 was prepared by spin-coating 12 wt % titanium diisopropoxide bis(acetylacetonate) in butanol on the fluorine-doped tin oxide (FTO) substrate (a). The flakes of TiO_2 nanotubes mixed with TiO_2 nanoparticles were spin-coated on the compact TiO_2 layer to form a TiO_2 nanoparticle/nanotube (TNN) film as an electron acceptor, electron transport, and light harvesting layer (b). The TiO_2 nanoparticles were prepared using TiO_2 paste (Ti-Nanoxide T/SP, solaronix) diluted in anhydrous ethanol. The TNN films were annealed at 500 °C for 1 h to improve crystallinity. The perovskite film was then coated onto the TNN film by a hot-casting technique at 90 °C, followed by annealing at 130 °C for 1 h (c). The hole-conductor layer of spiro-OMeTAD was formed on the active layer (d). The hole transport material was prepared with 73.52 mg of

spiro-OMeTAD (60 mMol), 17 µL of Li [bis-(trifluoromethanesulfonyl) imide] (Li-TFSI) solution (57.42 mg of Li-TFSI in 1 mL of acetonitrile), and 36.22 µL of 4-*tert*-bytylpyridine (500 mMol) in 1 mL of chlorobenzene. Finally, the top electrode of gold was formed by thermal evaporation (e). The energy band diagram of the perovskite solar cells with TiO_2 inclusion is as shown in Figure 1B. The band gap of the TNN film was similar to that of mesoporous TiO_2 film. The main role of the TNN film was to enhance light harvesting via the TiO_2 nanoparticles and/or nanotubes.

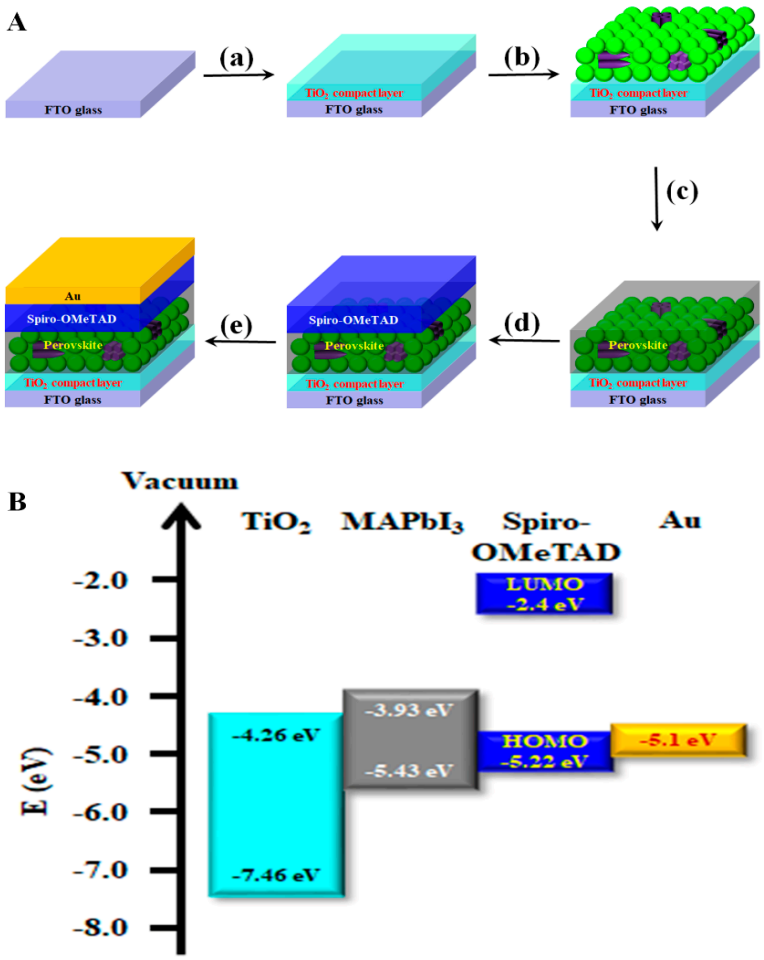

Figure 1. (**A**) Schematic illustration of fabrication processes of perovskite solar cells with TiO_2 films, including TiO_2 nanoparticles and flakes of TiO_2 nanotubes, and (**B**) an energy band diagram of the device.

2.4. Analysis

The photocurrent density-voltage (*J-V*) plots of the perovskite solar cells were measured using a Keithley series 2400 source meter (Tektronix, Beaverton, Portland, OR, USA) under AM1.5 illumination (100 mW/cm^2) provided by a 150-W Xenon solar simulator (Oriel Corp., model 91160A, Irvine, CA, USA). To examine the crystallinity of TiO_2 nanotubes, X-ray diffraction (XRD) analysis was performed with a Rigaku D/max-2500 (Rigaku Corp., Tokyo, Japan) using Cu Kα radiation. The absorption properties of the films were examined with ultraviolet-visible (UV-vis) spectroscopy using a JASCO(V-730) spectrometer (JSACO, Easton, MD, USA). The incident photon-to-current efficiency (IPCE) of the devices was measured using a monochromator coupled with a lock-in amplifier and a 500-W Xenon lamp (PV Measurements Inc., Model QEX7, Washington, DC, USA).

3. Results and Discussion

Figure 2 shows field emission scanning electron microscopy (FE-SEM) images of the TiO_2 nanotube arrays (Figure 2a,b) and the TNN film (Figure 2c,d). Pore diameter, wall thickness, interpore distance, and length of the TiO_2 nanotubes were approximately 100 nm, 20 nm, 200 nm, and 50 μm, respectively. Figure 2c exhibits the top view of the TiO_2 nanoparticle/nanotube (TNN) film formed on the FTO glass, which shows some flakes of TiO_2 nanotubes incorporated into the film. Figure 2d shows a cross-sectional SEM image of the perovskite solar cell configuration, obtained using a focused ion beam (FIB) method. The thickness of the TiO_2 compact layer, TNN layer, perovskite layer, hole-transport layer, and Au electrode were approximately 50 nm, 230 nm, 450 nm, 250 nm, and 260 nm, respectively.

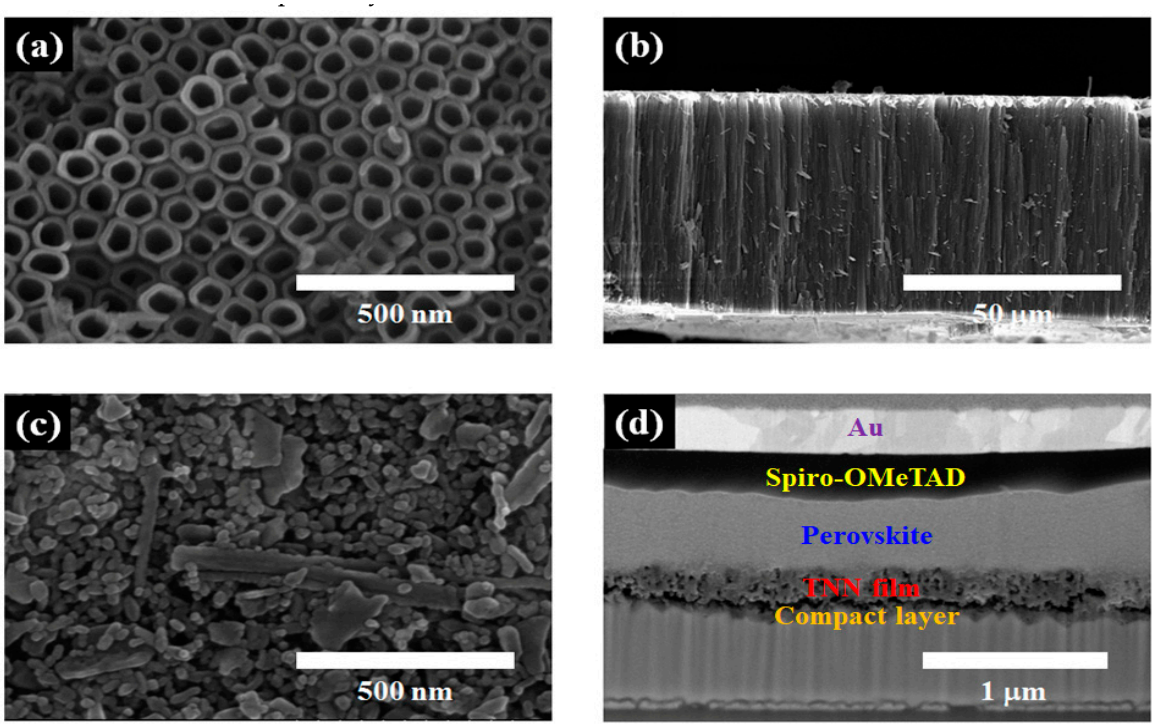

Figure 2. Field emission scanning electron microscopy (FE-SEM) images: (**a**) Top view and (**b**) cross-sectional view of TiO_2 nanotube arrays; (**c**) top view of TiO_2 nanoparticle/nanotube (TNN) film; (**d**) cross-sectional view of the perovskite solar cell structure, obtained via focused ion beam (FIB).

Figure 3 shows the X-ray diffraction (XRD) patterns of the TiO_2 nanotube arrays before and after thermal annealing at 500 °C for 1 h (Figure 3a) and the perovskite film on TiO_2/FTO (Figure 3b). The as-prepared TiO_2 nanotube arrays by anodization (black) were amorphous, but the annealed nanotubes (red) had crystalline phases of (101), (004), (200), (105), (211), and (118) at 2θ values of 25°, 38°, 48°, 53°, 55°, and 62°, respectively. A dominant peak at 25°, i.e., the (101) peak, was attributed to an anatase crystal phase (Figure 3a). The crystallinity and purity of the perovskite films were confirmed with strong peaks of (110) and (220) at 2θ values of 14° and 28°, respectively, without a $PbCl_2$ peak (Figure 3b), indicating that the tetragonal conformation of the perovskite structure was formed.

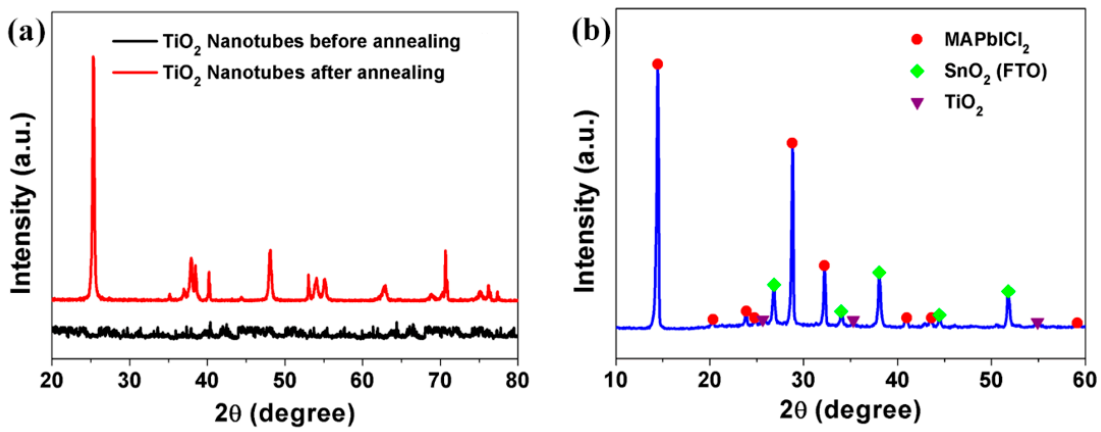

Figure 3. XRD patterns of (**a**) TiO_2 nanotube film before and after annealing and (**b**) perovskite film on TiO_2/fluorine-doped tin oxide (FTO).

Figure 4 shows photocurrent density-voltage (*J-V*) curves of the TNN-based perovskite solar cells as a function of weight percentage of TiO_2 nanotubes in the TNN-containing active layer. The corresponding photovoltaic parameters of the cells are summarized in Table 1. Compared to the TiO_2 nanoparticles only, the TNN-containing cells showed better performances with higher values of short circuit current density (J_{SC}), fill factor (*FF*), and power conversion efficiency (η). The optimal content of TiO_2 nanotubes in TNNs was 9 wt %, resulting in 0.886 V of V_{oc}, 25.5'mA/cm^2 of J_{SC}, 67.9% of *FF*, and 15.335% of η. More interestingly, the TNN-containing cells showed a substantial increase in J_{SC}, from 23.9 mA/cm^2 without nanotubes to 25.5 mA/cm^2 with 9 wt % nanotubes, suggesting that the micronmeter-sized TiO_2 nanotubes enhanced the charge carrier generation by harvesting more sunlight, probably attributed to the Mie scattering effect. To check the stability of TNN-based PSCs, we exposed the devices without encapsulation to an Ar environment at room temperature. Figure S1 (Supplementary Materials) shows V_{oc}, J_{SC}, *FF*, and η from the *J-V* test results for 80 days. Overall, the photovoltaic parameters of the devices were stabilized after 40 days and sustained their stability over 80 days, while retaining 95%–99% of their original values. To evaluate the reproducibility of the TNN-based PSCs, we fabricated 20 devices and measured device performance. Figure S2 shows the histogram of the power conversion efficiency distribution for 20 devices, apparently presenting the best performance of the PSCs with 9 wt % of TiO_2 nanotubes, i.e., η = 14%–15%.

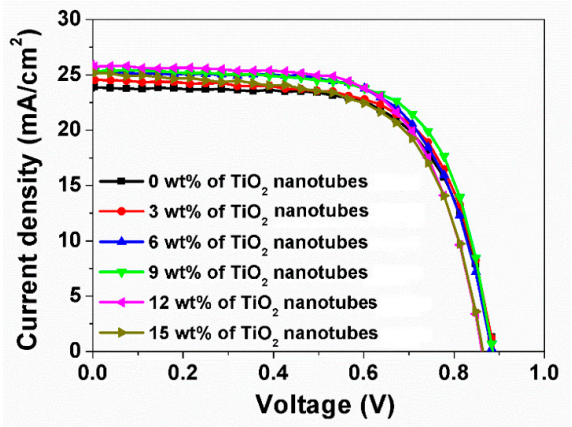

Figure 4. Current density-Voltage (*I-V*) curves of perovskite solar cells with 0, 3, 6, 9, 12, and 15 wt % of TiO_2 nanotube arrays in a TiO_2 composite film.

Table 1. Photovoltaic properties of perovskite solar cells with 0, 3, 6, 9, 12, and 15 wt % of TiO_2 nanotube arrays in a TiO_2 composite film.

	V_{oc} (V)	J_{SC} (mA/cm^2)	*FF* (%)	η (%)
0 wt %	0.888	23.908	66.694	14.162
3 wt %	0.888	24.705	66.018	14.489
6 wt %	0.884	25.307	66.330	14.834
9 wt %	0.886	25.500	67.906	15.335
12 wt %	0.863	25.888	65.744	14.684
15 wt %	0.865	25.223	63.996	13.960

To confirm the light harvesting effect of TiO_2 nanotube flakes in the active layer, the reflectance spectra of the TNN films and the IPCE spectra of the TNN-containing perovskite solar cells were measured. Figure 5 shows the normalized reflectance spectra in the TNN films as a function of weight percentage of TiO_2 nanotubes. As the content of TiO_2 nanotubes increased, the TNN films showed a similar trend of reflectance, but with some variation in intensity. At wavelengths greater than 570 nm, the intensity of the reflectance decreased with the amount of the TiO_2 nanotubes, indicating more light harvesting by TiO_2 nanotubes at longer wavelengths (i.e., 570–800 nm), thus enhancing charge carrier generation in the active layer.

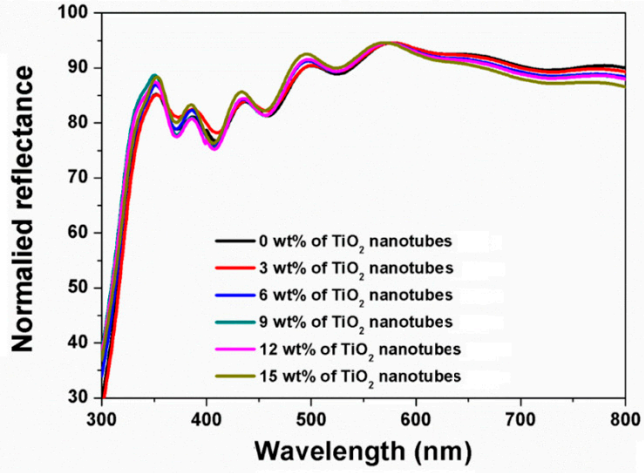

Figure 5. Normalized reflectance spectra of TiO_2 composite films with 0, 3, 6, 9, 12, and 15 wt % of TiO_2 nanotubes.

Figure 6 shows the normalized IPCE spectra from TNN-containing perovskite solar cells with varying content of the TiO_2 nanotubes from 0 to 15 wt %. With increasing amounts of TiO_2 nanotubes, the photon-to-current efficiency increased substantially at wavelengths greater than 570 nm, which was in good agreement with Figures 4 and 5, attributed to more light harvesting due to a scattering effect by nanotubes and more generation of charge carriers in the active layer. However, it is worthwhile to note that the incorporation of nanotubes of more than 12 wt % increased the recombination rate and thus decreased the photocurrent density that affected *FF* and V_{oc} (also see Table 1). Generally, it is known that according to Rayleigh theory, scattering by TiO_2 nanoparticles of 20–30 nm is very weak [51,54]. The pore diameter of TiO_2 nanotubes was 100 nm (Figure 2a), and the length of nanotubes in the TNN film was in the range of 300–1000 nm in size (Figure 2c): Thus, the enhancement of light harvesting with the TNN films was probably attributed to the Mie scattering effect. In addition, as the TNN films were mesoporous, perovskite solution easily penetrated into the TNN film layer. Thus, it is believed that scattering was toward the perovskite as well as in the direction of the tubes.

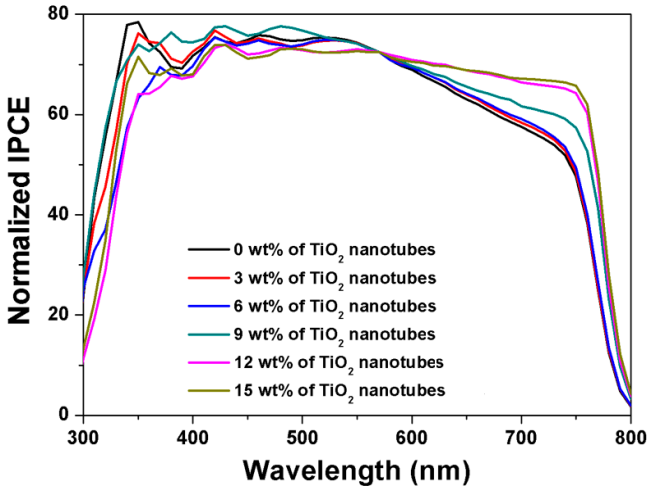

Figure 6. Normalized incident photon-to-current efficiency (IPCE) spectra of perovskite solar cells with 0, 3, 6, 9, 12, and 15 wt % of TiO_2 nanotubes in the active layer.

4. Conclusions

Perovskite solar cells were fabricated with the inclusion of TiO_2 nanoparticles/nanotubes as light harvesting materials and were characterized in terms of the normalized reflectance and IPCE. The TiO_2 nanoparticle/nanotube-based cells harvested more sunlight with the content of the nanotubes (attributed to the Mie scattering effect) and thus enhanced the carrier charge generation and conduction. However, a large amount of TiO_2 nanotubes did not result in improved energy conversion efficiency because of high levels of recombination and low electron density in the active layer. With the optimal content of the TiO_2 nanotubes (i.e., 9 wt %), the devices showed high photocurrent density and a power conversion efficiency of 15.34%. The TNN-based PSCs also showed good stability, retaining 95–99% of their initial photovoltaic parameter values. The obtained results could be applicable to different types of solar cells and photocatalysts and water splitting technology for hydrogen generation.

Supplementary Materials: The following are available online at http://www.mdpi.com/2079-4991/9/3/326/s1, Figure S1: The stability of perovskite solar cells with 9wt% of TiO_2 nanotubes in a TiO_2 composite film, Figure S2: The histograms of PCE with 0, 9 and 15wt% of TiO_2 nanotubes in active layer.

Author Contributions: H.-Y.Y. and S.K.L. designed and performed experiments. S.H.K and W.-Y.R. helped in measurements, data acquisition, and analysis. W.-Y.R. and Y.-B.H. co-wrote the manuscript. Y.-B.H. was responsible for project planning and funding. Correspondence and requests for materials should be addressed to Y.-B.H. All authors read and approved the final manuscript.

Funding: This paper was supported by research funds from Chonbuk National University in 2017.

Conflicts of Interest: The authors declare no conflicts of interest. The founding sponsors had no role in the design of the study; in the collection, analyses, or interpretation of data; in the writing of the manuscript; or in the decision to publish the results.

References

1. Wang, Y.; Mahmoudi, T.; Yang, H.-Y.; Bhat, K.S.; Yoo, J.-Y.; Hahn, Y.-B. Fully-ambient-processed mesoscopic semitransparent perovskite solar cells by islands-structure-$MAPbI_{3-x}Cl_x$-NiO composite and Al_2O_3/NiO interface engineering. *Nano Energy* **2018**, *49*, 59–66. [CrossRef]
2. Mahmoudi, T.; Wang, Y.; Hahn, Y.-B. Graphene and its derivatives for solar cells application. *Nano Energy* **2018**, *47*, 51–65. [CrossRef]
3. Wang, Y.; Mahmoudi, T.; Rho, W.-Y.; Yang, H.-Y.; Seo, S.; Bhat, K.S.; Ahmad, R.; Hahn, Y.-B. Ambient-air-solution-processed efficient and highly stable perovskite solar cells based on $CH_3NH_3PbI_{3-x}Cl_x$-NiO composite with Al_2O_3/NiO interfacial engineering. *Nano Energy* **2017**, *40*, 408–417. [CrossRef]

4. Mahmoudi, T.; Seo, S.; Yang, H.-Y.; Rho, W.-Y.; Wang, Y.; Hahn, Y.-B. Efficient bulk heterojunction hybrid solar cells with graphene-silver nanoparticles composite synthesized by microwave-assisted reduction. *Nano Energy* **2016**, *28*, 179–187. [CrossRef]
5. Wang, Y.; Rho, W.-Y.; Yang, H.-Y.; Mahmoudi, T.; Seo, S.; Lee, D.-H.; Hahn, Y.-B. Air-stable, hole-conductor-free high photocurrent perovskite solar cells with $CH_3NH_3PbI_3$–NiO nanoparticles composite. *Nano Energy* **2016**, *27*, 535–544. [CrossRef]
6. Kojima, A.; Teshima, K.; Shirai, Y.; Miyasaka, T. Organometal Halide Perovskites as Visible-Light Sensitizers for Photovoltaic Cells. *J. Am. Chem. Soc.* **2009**, *131*, 6050–6051. [CrossRef] [PubMed]
7. Im, J.-H.; Lee, C.-R.; Lee, J.-W.; Park, S.-W.; Park, N.-G. 6.5% efficient perovskite quantum-dot-sensitized solar cell. *Nanoscale* **2011**, *3*, 4088–4093. [CrossRef] [PubMed]
8. Lee, M.M.; Teuscher, J.; Miyasaka, T.; Murakami, T.N.; Snaith, H.J. Efficient hybrid solar cells based on meso-superstructured organometal halide perovskites. *Science* **2012**, *338*, 643–647. [CrossRef] [PubMed]
9. Etgar, L.; Gao, P.; Xue, Z.; Peng, Q.; Chandiran, A.K.; Liu, B.; Nazeeruddin, M.K.; Gratzel, M. Mesoscopic $CH_3NH_3PbI_3/TiO_2$ heterojunction solar cells. *J. Am. Chem. Soc.* **2012**, *134*, 17396–17399. [CrossRef] [PubMed]
10. Burschka, J.; Pellet, N.; Moon, S.J.; Humphry-Baker, R.; Gao, P.; Nazeeruddin, M.K.; Gratzel, M. Sequential deposition as a route to high-performance perovskite-sensitized solar cells. *Nature* **2013**, *499*, 316–319. [CrossRef] [PubMed]
11. Nie, W.; Tsai, H.; Asadpour, R.; Blancon, J.-C.; Neukirch, A.J.; Gupta, G.; Crochet, J.J.; Chhowalla, M.; Tretiak, S.; Alam, M.A.; et al. High-efficiency solution-processed perovskite solar cells with millimeter-scale grains. *Science* **2015**, *347*, 522–525. [CrossRef] [PubMed]
12. Kazim, S.; Nazeeruddin, M.K.; Gratzel, M.; Ahmad, S. Perovskite as light harvester: A game changer in photovoltaics. *Angew. Chem. Int. Ed. Engl.* **2014**, *53*, 2812–2824. [CrossRef] [PubMed]
13. Xing, G.; Mathews, N.; Sun, S.; Lim, S.S.; Lam, Y.M.; Gratzel, M.; Mhaisalkar, S.; Sum, T.C. Long-range balanced electron- and hole-transport lengths in organic-inorganic $CH_3NH_3PbI_3$. *Science* **2013**, *342*, 344–347. [CrossRef] [PubMed]
14. Mitzi, D.B.; Feild, C.; Harrison, W.; Guloy, A. Conducting tin halides with a layered organic-based perovskite structure. *Nature* **1994**, *369*, 467–469. [CrossRef]
15. Poglitsch, A.; Weber, D. Dynamic disorder in methylammoniumtrihalogenoplumbates (II) observed by millimeter-wave spectroscopy. *J. Chem. Phys.* **1987**, *87*, 6373–6378. [CrossRef]
16. Im, J.-H.; Chung, J.; Kim, S.-J.; Park, N.-G. Synthesis, structure, and photovoltaic property of a nanocrystalline 2H perovskite-type novel sensitizer ($CH_3CH_2NH_3$) PbI_3. *Nanoscale Res. Lett.* **2012**, *7*, 1–7. [CrossRef] [PubMed]
17. Baikie, T.; Fang, Y.; Kadro, J.M.; Schreyer, M.; Wei, F.; Mhaisalkar, S.G.; Graetzel, M.; White, T.J. Synthesis and crystal chemistry of the hybrid perovskite $(CH_3NH_3)PbI_3$ for solid-state sensitised solar cell applications. *J. Mater. Chem. A* **2013**, *1*, 5628. [CrossRef]
18. Stranks, S.D.; Eperon, G.E.; Grancini, G.; Menelaou, C.; Alcocer, M.J.; Leijtens, T.; Herz, L.M.; Petrozza, A.; Snaith, H.J. Electron-hole diffusion lengths exceeding 1 micrometer in an organometal trihalide perovskite absorber. *Science* **2013**, *342*, 341–344. [CrossRef] [PubMed]
19. Heo, J.H.; Im, S.H.; Noh, J.H.; Mandal, T.N.; Lim, C.-S.; Chang, J.A.; Lee, Y.H.; Kim, H.-j.; Sarkar, A.; Nazeeruddin, M.K.; et al. Efficient inorganic–organic hybrid heterojunction solar cells containing perovskite compound and polymeric hole conductors. *Nat. Photonics* **2013**, *7*, 486–491. [CrossRef]
20. Jeon, N.J.; Lee, H.G.; Kim, Y.C.; Seo, J.; Noh, J.H.; Lee, J.; Seok, S.I. o-Methoxy substituents in spiro-OMeTAD for efficient inorganic-organic hybrid perovskite solar cells. *J. Am. Chem. Soc.* **2014**, *136*, 7837–7840. [CrossRef] [PubMed]
21. Ye, S.; Sun, W.; Li, Y.; Yan, W.; Peng, H.; Bian, Z.; Liu, Z.; Huang, C. CuSCN-Based Inverted Planar Perovskite Solar Cell with an Average PCE of 15.6%. *Nano Lett.* **2015**, *15*, 3723–3728. [CrossRef] [PubMed]
22. Edri, E.; Kirmayer, S.; Cahen, D.; Hodes, G. High open-circuit voltage solar cells based on organic–inorganic lead bromide perovskite. *J. Phys. Chem. Lett.* **2013**, *4*, 897–902. [CrossRef] [PubMed]
23. Ball, J.M.; Lee, M.M.; Hey, A.; Snaith, H.J. Low-temperature processed meso-superstructured to thin-film perovskite solar cells. *Energy Environ. Sci.* **2013**, *6*, 1739. [CrossRef]
24. Noh, J.H.; Jeon, N.J.; Choi, Y.C.; Nazeeruddin, M.K.; Grätzel, M.; Seok, S.I. Nanostructured $TiO_2/CH_3NH_3PbI_3$ heterojunction solar cells employing spiro-OMeTAD/Co-complex as hole-transporting material. *J. Mater. Chem. A* **2013**, *1*, 11842. [CrossRef]

25. Wang, K.C.; Jeng, J.Y.; Shen, P.S.; Chang, Y.C.; Diau, E.W.; Tsai, C.H.; Chao, T.Y.; Hsu, H.C.; Lin, P.Y.; Chen, P.; et al. p-type Mesoscopic Nickel Oxide/Organometallic Perovskite Heterojunction Solar Cells. *Sci. Rep.* **2014**, *4*, 4756. [CrossRef] [PubMed]
26. Hagfeldt, A.; Boschloo, G.; Sun, L.; Kloo, L.; Pettersson, H. Dye-sensitized solar cells. *Chem. Rev.* **2010**, *110*, 6595–6663. [CrossRef] [PubMed]
27. Kay, A.; Gratzel, M. Dye-Sensitized Core-Shell Nanocrystals: Improved Efficiency of Mesoporous Tin Oxide Electrodes Coated with a Thin Layer of an Insulating Oxide. *Chem. Mater.* **2002**, *14*, 2930–2935. [CrossRef]
28. Kim, H.-S.; Im, S.H.; Park, N.-G. Organolead Halide Perovskite: New Horizons in Solar Cell Research. *J. Phys. Chem. C* **2014**, *118*, 5615–5625. [CrossRef]
29. O'regan, B.; Grfitzeli, M. A low-cost, high-efficiency solar cell based on dye-sensitized. *Nature* **1991**, *353*, 737–740. [CrossRef]
30. Yang, Z.; Pan, J.; Liang, Y.; Li, Q.; Xu, D. Ambient Air Condition for Room-Temperature Deposition of $MAPbI_3$ Films in Highly Efficient Solar Cells. *Small* **2018**, *14*, 1802240. [CrossRef] [PubMed]
31. Bella, F.; Renzi, P.; Cavallo, C.; Gerbaldi, C. Caesium for perovskite solar cells: An overview. *Chem. Eur. J.* **2018**, *24*, 12183–12205. [CrossRef] [PubMed]
32. Abate, A.; Correa-Baena, J.P.; Saliba, M.; Su'ait, M.S.; Bella, F. Perovskite solar cells: From the laboratory to the assembly line. *Chem. Eur. J.* **2018**, *24*, 3083–3100. [CrossRef] [PubMed]
33. Wang, B.; Zhu, X.; Li, S.; Chen, M.; Lu, H.; Yang, Y. Ag@ SiO_2 core-shell nanoparticles embedded in a TiO_2 mesoporous layer substantially improve the performance of perovskite solar cells. *Nanomaterials* **2018**, *8*, 701. [CrossRef] [PubMed]
34. Wu, Y.; Chen, W.; Chen, G.; Liu, L.; He, Z.; Liu, R. The Impact of Hybrid Compositional Film/Structure on Organic–Inorganic Perovskite Solar Cells. *Nanomaterials* **2018**, *8*, 356. [CrossRef] [PubMed]
35. Chen, L.; Zhang, H.; Zhang, J.; Zhou, Y. A Compact and Smooth $CH_3NH_3PbI_3$ Film: Investigation of Solvent Sorts and Concentrations of CH_3NH_3I towards Highly Efficient Perovskite Solar Cells. *Nanomaterials* **2018**, *8*, 897. [CrossRef] [PubMed]
36. Mahmoudi, T.; Wang, Y.; Hahn, Y.-B. Stability Enhancement in Perovskite Solar Cells with Perovskite/Silver–Graphene Composites in the Active Layer. *ACS Energy Lett.* **2018**, *4*, 235–241. [CrossRef]
37. Nie, R.; Mehta, A.; Park, B.-w.; Kwon, H.-W.; Im, J.; Seok, S.I. Mixed sulfur and iodide-based lead-free perovskite solar cells. *J. Am. Chem. Soc.* **2018**, *140*, 872–875. [CrossRef] [PubMed]
38. Mor, G.K.; Shankar, K.; Paulose, M.; Varghese, O.K.; Grimes, C.A. Use of highly-ordered TiO_2 nanotube arrays in dye-sensitized solar cells. *Nano Lett.* **2006**, *6*, 215–218. [CrossRef] [PubMed]
39. Rho, W.-Y.; Kim, H.-S.; Chung, W.-J.; Suh, J.S.; Jun, B.-H.; Hahn, Y.-B. Enhancement of power conversion efficiency with TiO_2 nanoparticles/nanotubes-silver nanoparticles composites in dye-sensitized solar cells. *Appl. Surf. Sci.* **2018**, *429*, 23–28. [CrossRef]
40. Zhu, K.; Neale, N.R.; Miedaner, A.; Frank, A.J. Enhanced charge-collection efficiencies and light scattering in dye-sensitized solar cells using oriented TiO_2 nanotubes arrays. *Nano Lett.* **2007**, *7*, 69–74. [CrossRef] [PubMed]
41. Adachi, M.; Murata, Y.; Okada, I.; Yoshikawa, S. Formation of titania nanotubes and applications for dye-sensitized solar cells. *J. Electrochem. Soc.* **2003**, *150*, 488–493. [CrossRef]
42. Rho, W.-Y.; Song, D.H.; Lee, S.H.; Jun, B.-H.J.N. Enhanced Efficiency in Dye-Sensitized Solar Cells by Electron Transport and Light Scattering on Freestanding TiO_2 Nanotube Arrays. *Nanomaterials* **2017**, *7*, 345. [CrossRef] [PubMed]
43. Gong, D.; Grimes, C.A.; Varghese, O.K.; Hu, W.; Singh, R.; Chen, Z.; Dickey, E.C. Titanium oxide nanotube arrays prepared by anodic oxidation. *J. Mater. Res.* **2001**, *16*, 3331–3334. [CrossRef]
44. Mor, G.K.; Varghese, O.K.; Paulose, M.; Shankar, K.; Grimes, C.A. A review on highly ordered, vertically oriented TiO_2 nanotube arrays: Fabrication, material properties, and solar energy applications. *Sol. Energy Mater. Sol. Cells* **2006**, *90*, 2011–2075. [CrossRef]
45. Paulose, M.; Prakasam, H.E.; Varghese, O.K.; Peng, L.; Popat, K.C.; Mor, G.K.; Desai, T.A.; Grimes, C.A. TiO_2 nanotube arrays of 1000 μm length by anodization of titanium foil: Phenol red diffusion. *J. Phys. Chem. C* **2007**, *111*, 14992–14997. [CrossRef]
46. Rho, C.; Min, J.-H.; Suh, J.S. Barrier layer effect on the electron transport of the dye-sensitized solar cells based on TiO_2 nanotube arrays. *J. Phys. Chem. C* **2012**, *116*, 7213–7218. [CrossRef]

47. Kasuga, T.; Hiramatsu, M.; Hoson, A.; Sekino, T.; Niihara, K. Formation of titanium oxide nanotube. *Langmuir* **1998**, *14*, 3160–3163. [CrossRef]
48. Chen, Q.; Zhou, W.; Du, G.; Peng, L.-M. Trititanate nanotubes made via a single alkali treatment. *Adv. Mater.* **2002**, *14*, 1208–1211. [CrossRef]
49. Yao, B.; Chan, Y.; Zhang, X.; Zhang, W.; Yang, Z.; Wang, N. Formation mechanism of TiO_2 nanotubes. *Appl. Phys. Lett.* **2003**, *82*, 281–283. [CrossRef]
50. Rho, C.; Suh, J.S. Filling TiO_2 nanoparticles in the channels of TiO_2 nanotube membranes to enhance the efficiency of dye-sensitized solar cells. *Chem. Phys. Lett.* **2011**, *513*, 108–111. [CrossRef]
51. Zhang, Q.; Myers, D.; Lan, J.; Jenekhe, S.A.; Cao, G. Applications of light scattering in dye-sensitized solar cells. *Phys. Chem. Chem. Phys.* **2012**, *14*, 14982–14998. [CrossRef] [PubMed]
52. Hore, S.; Nitz, P.; Vetter, C.; Prahl, C.; Niggemann, M.; Kern, R. Scattering spherical voids in nanocrystalline TiO_2–enhancement of efficiency in dye-sensitized solar cells. *Chem. Commun.* **2005**, 2011–2013. [CrossRef] [PubMed]
53. Deepak, T.; Anjusree, G.; Thomas, S.; Arun, T.; Nair, S.V.; Nair, A.S. A review on materials for light scattering in dye-sensitized solar cells. *RSC Adv.* **2014**, *4*, 17615–17638. [CrossRef]
54. Huang, F.; Chen, D.; Zhang, X.L.; Caruso, R.A.; Cheng, Y.B. Dual-Function Scattering Layer of Submicrometer-Sized Mesoporous TiO_2 Beads for High-Efficiency Dye-Sensitized Solar Cells. *Adv. Funct. Mater.* **2010**, *20*, 1301–1305. [CrossRef]